Received 25 May 2022, accepted 15 June 2022, date of publication 20 June 2022, date of current version 27 July 2022.

Digital Object Identifier 10.1109/ACCESS.2022.3184424

Effect of GIC Neutral Blocking Devices (NBDs) on Power Network Ferroresonance in Malaysia

ZMNAKO MOHAMMED KHURSHID[1], NUR FADILAH AB AZIZ[1], (Member, IEEE), ZETI AKMA RHAZALI[1], AND MOHD ZAINAL ABIDIN AB KADIR[2], (Senior Member, IEEE)

[1]College of Engineering, Institute of Power Engineering (IPE), Universiti Tenaga Nasional, Kajang, Selangor 43000, Malaysia
[2]Advanced Lightning, Power and Energy Research Centre (ALPER), Faculty of Engineering, Universiti Putra Malaysia, Serdang, Selangor 43400, Malaysia

Corresponding author: Zmnako Mohammed Khurshid (zmnako24@hotmail.com)

This work was supported in part by the Ministry of Higher Education (MOHE) of Malaysia under Grant 20180112FRGS, and in part by the Universiti Tenaga Nasional through the Universiti Tenaga Nasional (UNITEN) Bold Grant.

ABSTRACT Geomagnetic disturbance (GMD) arises during space weather and solar activity can result in geomagnetically induced current (GIC) flow in the grounded power transformers in the power network. This GIC may cause half-cycle saturation of transformers and lead to severe damage or blackout. To block the GIC flow into the power transformers, the neutral blocking devices (NBDs) based on capacitor banks are often installed in the neutral ground paths of transformers to mitigate the GIC. However, the high voltage (HV) can build up across these capacitors during ground faults and may cause a ferroresonance phenomenon in the power network. This phenomenon generates high voltages/currents in the transformer windings and results in transformer failure. This work investigates the effect of connected NBDs to the power transformers on the potential power network ferroresonance in Peninsular Malaysia. The complete analysis was carried out using the Power System Computer-Aided Design for Electromagnetic Transients including Direct Current (PSCAD/EMTDC) software. These transformers were selected in the power network due to the sensitivity of their locations to GMD events. The NBD systems were tested under different working conditions. The simulation results found that the metal oxide varistors (MOVs) arresters in NBDs fault protection mode effectively clamped ferroresonance overvoltages below the protection level under faulty conditions. Also, the results showed that GIC protection modes with 1 Ω and 3180 μF in the mitigation systems had the lowest ferroresonance overvoltages in the neutrals of the transformers under faulty conditions. Based on the results, the recommendations were provided to the local power utility which will help to improve the reliability of the power supply to the consumers.

INDEX TERMS Neutral blocking devices, ferroresonance, overvoltage, Malaysian power network, PSCAD/EMTDC, power transformer.

I. INTRODUCTION

Geomagnetically induced current (GIC) is a phenomenon that arises as a result of Geomagnetic Disturbance (GMD) during solar storms and space weather events [1], [2]. When these storms strike the Earth's magnetic field, rapid magnetic field variations occur on the ground and produce a geoelectric field on the surface of the Earth [2]–[4]. This geoelectric field induces quasi-DC current or GIC flow through conductors and ground connected technological infrastructure [2]–[6]. Power transformers are the most affected by the GIC [7], [8]. When the GIC flows into the windings of the transformer, the asymmetrical saturation generated in the transformer magnetic cores is called half-cycle saturation [9], [10]. This saturation extremely increases the reactive power losses and harmonic distortion of the transformer [11] and could result in long-term damage to the system's components [12], [13] or blackout [8], [14], [15].

Researchers have developed different mitigation approaches to limit the GIC flow into the power network. The neutral blocking devices (NBDs) based on the capacitor banks are the most common and attractive solutions to mitigate the GIC in power systems [16]. Although the connection of the capacitor in the neutral ground point of the transformer limits the flow of the GIC into the winding of a transformer, the high voltage (HV) could build up across the capacitor banks and

The associate editor coordinating the review of this manuscript and approving it for publication was Giambattista Gruosso.

lead to ferroresonance overvoltage conditions. The ferroresonance phenomenon is a non-linear resonance that occurs in electric circuits containing non-linear inductance, capacitance, and a voltage source. Non-linear inductance and capacitance include power transformers, voltage transformers, long transmission lines and capacitor banks [17]–[19]. Usually, this phenomenon is observed during transient disturbances like high phase to ground faults [20]–[22], lightning strikes [18], switching or the series connections of the capacitors with transformer magnetising impedance and removing the loads at the end of the transmission line [23], [24].

The ferroresonance can cause overvoltages, overcurrents, and distorted voltage and current waveforms in an electrical power system, posing a risk to transmission and distribution equipment [25], [26], like overheating a transformer and possible insulation damage, failures in cables, and arresters [8], [19], [23]. As a result of these effects, great care must be considered in the design of the GIC mitigation systems. The strategy must be carefully examined to avoid problems in the operation of the power system [27], [28]. In addition, the overvoltage magnitudes due to ground faults depend on the system grounding method (i.e., solidly grounded, resistance grounded, high resistance grounded or ungrounded systems) [29]. Therefore, this research investigates the effect of GIC NBD systems on the potential power network ferroresonance in Peninsular Malaysia. In the previous work, these NBDs were connected to the four HV power transformer types in the Malaysian power network. The efficacy of these mitigation devices has been tested under GIC condition.

These transformer types have been selected from the power network due to the sensitivity of their locations to GMD events. The connected NBDs could successfully block the injected GICs in the neutral paths of transformers [30]. In this work, these NBD systems will be tested under the faulty condition to investigate their impacts on the potential power network ferroresonance. A complete system was modelled using the Power System Computer-Aided Design for Electromagnetic Transients including Direct Current (PSCAD/EMTDC) software. The PSCAD/EMTDC is a time-domain industry-standard simulation tool used to study the electromagnetic transient behaviour of electrical systems [31] which is commercially available online [32]. Its graphical user interface enables all simulation aspects to be conducted within a single integrated environment including circuit assembly, simulation-time control, result analysis, and reporting. This paper is divided into the following sections. The second section presents the modelling design of the system which includes the NBD systems. In the third section, the results of the simulation cases are presented. Finally, the fourth section presents the conclusion and recommendations to the local power utility in Malaysia.

II. MODELLING DESIGN OF THE SYSTEM

The Malaysian power network and GIC mitigation system based on the NBD were modelled using PSCAD/EMTDC software. The power network model includes 54 substations

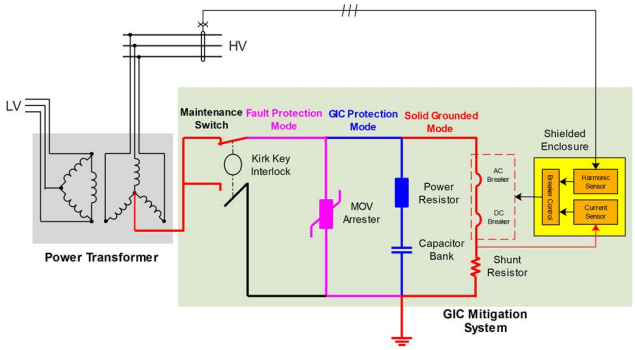

FIGURE 1. GIC mitigation system based on NBD.

and 138 buses which are interconnected through transmission lines at voltages of 500 kV, 275 kV, and 132 kV. The GIC mitigation system was modelled based on a conventional NBD concept presented in [20], [21]. It consists of three operational modes which are solid ground, GIC protection and ground fault protection modes, as presented in Fig. 1. The solid ground mode is modelled by an AC breaker and a DC disconnect breaker connected in series through a shunt resistor (0.001 Ω) to the ground. The breakers are built in the PSCAD/EMTDC model with different options. The option "open possible at any current" at the AC ground switch was disabled, and the current chopping limit was set at zero. The DC disconnect switch is modelled and enabled to open at any current. The AC breaker has an HV stand-off used to protect a DC breaker from any overvoltages, and a DC breaker is used to break DC and quasi-DC currents.

GIC protection mode comprises of 50 kW (1 Ω) power resistor connected in series with 1 Ω impedance capacitor bank to ground, the capacitor value is equal to (3180 μF) at 50 Hz calculated based on Equation 2.

$$Xc = \frac{1}{2\pi fC} = 1 \tag{1}$$

$$C = \frac{1}{2\pi fXc} \tag{2}$$

$$C = \frac{1}{2\pi \times 50 \times 1} \approx 3180\ \mu F \tag{3}$$

In the previous work, we tested the GIC protection mode in the connected NBD systems under an extreme geomagnetic storm scenario with the value of 20 V/km. The capacitor banks in the NBDs successfully could block the induced GICs in the neutral paths of four types of HV power transformers, as presented in Table 1 [30]. In this study, NBD systems were tested under the faulty condition to investigate the impacts of the GIC protection mode in the system on the potential power network ferroresonance and the effectiveness of the fault protection mode in suppressing the resonance overvoltages. Note that the effect of the rest of the network on the short-circuit current was ignored in the current analysis in order to minimise the manuscript size and avoid confusion to the reader. The flowchart of the used method is illustrated in Fig. 2.

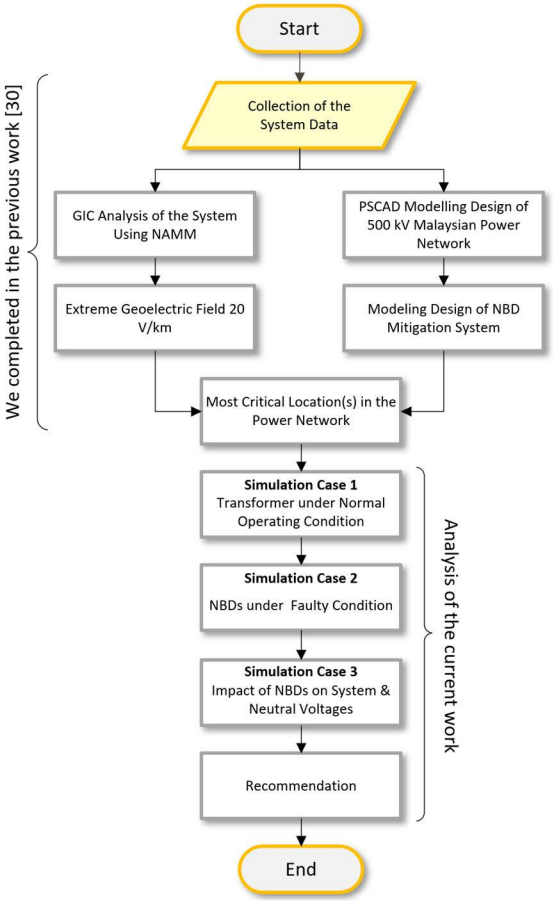

FIGURE 2. The flowchart of the used method.

The fault protection mode includes a 4 kV metal oxide varistor (MOV) surge arrester is used to protect the capacitor bank in the NBD system and transformer from any resonance overvoltage that might occur across the capacitor during any line to ground faults. The protection level of the arrester was set to 3.67 kV. The non-linear I–V characteristics curve of the MOV arrester is presented in Fig. 3.

Varistors are variable resistors with varying resistivity that corresponds to the applied voltage. They consist of materials that present highly non-linear I–V characteristics, such as zinc oxide with admixtures of other metal oxides. The I–V characteristics of MOVs are significant parameters of the surge arrester. MOV arresters are used to protect small, medium, and high-voltage systems against transient overvoltage. They also provide high resistance under normal operation (normally above 1 MΩ). When a transient surge occurs, their resistance decreases rapidly to below 1 Ω within a few nanoseconds and the applied transient current is discharged to the ground. Furthermore, MOVs provide a fast response to transient surges and high energy dissipation characteristics. Nevertheless, their life expectancy is limited as they are degraded when exposed to a few large surges or much smaller surges [33].

To ensure the accuracy of the I–V characteristics and clamping level of the used arrester, the 10/350 μs 25 kA

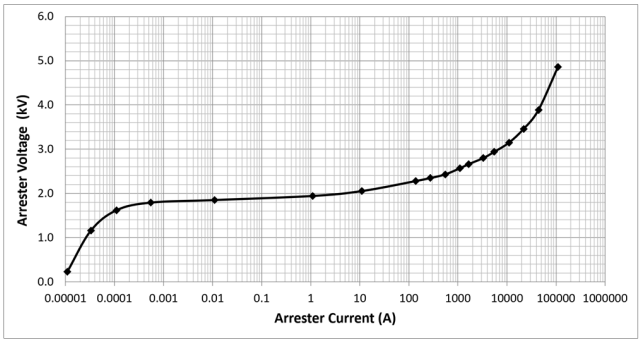

FIGURE 3. I–V characteristics of 4 kV surge arrester.

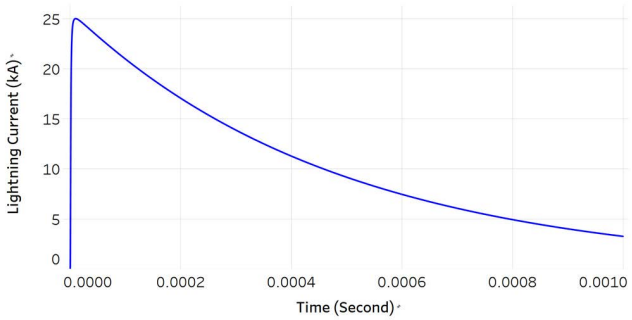

FIGURE 4. 10/350 μs 25 kA lightning current waveform.

standard lightning current waveform was applied to the arrester in the PSCAD. The lightning current was modelled using the Heidler function based on the following Equation.

$$i(t) = \frac{I_0}{\eta} \cdot \frac{\left(\frac{t}{\tau_1}\right)^n}{1 + \left(\frac{t}{\tau_1}\right)^n} exp^{\left(-\frac{t}{\tau_2}\right)} \quad (4)$$

where I_0 is the current peak value, η is the correction factor, τ_1 is the rise time, and τ_2 is the decay time. The lightning current waveform and the clamping voltage of the MOV arrester are shown in Figs. 4 and 5, respectively.

III. RESULTS AND DISCUSSION

In this section, three case studies were performed, including power transformers under normal operating conditions, NBDs under faulty conditions, and the impact of NBDs on the system and neutral voltages. The locations of these connected NBDs to the transformers in the system were selected based on their vulnerability to the GICs, as illustrated in Fig. 2. The details of these simulation cases are presented and discussed in the following subsections, respectively.

A. RESULTS OF SIMULATION CASE 1

In this case study, the PSCAD model of the Malaysian power network was operated under steady-state conditions. The results of RMS and instantaneous voltages and current waveforms of four types of HV transformers that were connected to NBDs in the power network are illustrated in Figs. 6 and 7. According to Fig. 6, the RMS voltages of the transformers

TABLE 1. Details of transformers that are connected to NBD systems.

Type	Rated Voltage (kV)	Rated MVA	Substation No.
Autotransformer	500/275	1050	21
Autotransformer	275/132	180	22
Standard Transformer	132/33	45	17
Standard Transformer	132/11	30	19

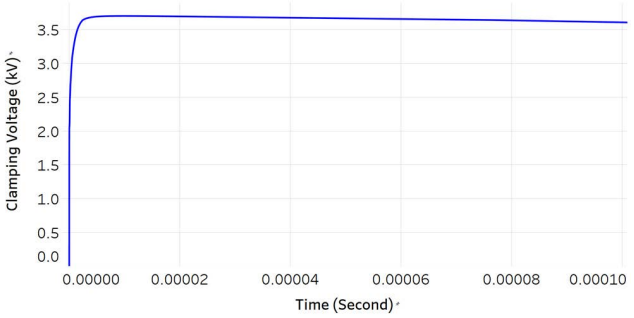

FIGURE 5. Clamping voltage of 4 kV MOV arrester.

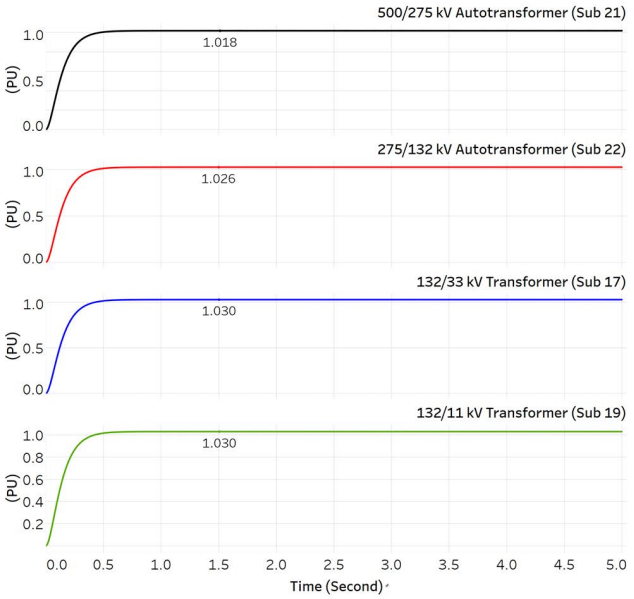

FIGURE 6. RMS voltages at the primary sides of different transformer types in the Malaysian power network under steady-state conditions.

were within the acceptable limits of the voltage regulation in Malaysia, which were close to 1 pu [34]–[36].

It was obvious from the figure that the system reached a steady-state condition after 0.7 seconds of the simulation time. Fig. 7 presents the sinusoidal current and voltage waveforms at the primary sides of the transformers under steady-state conditions.

Based on the figure, the output current and voltage profiles of the power transformers were pure (clean) three-phase sinewave and symmetrical around zero. Note that the peak values of the voltages presented in the figure are instantaneous phase to ground quantities provided by multimeters in the PSCAD. The peak value of voltage waveform at the primary side of 500/275 kV autotransformer is calculated according to Equation 6.

$$V_{phase} = \frac{500}{\sqrt{3}} = 288.68\ kV \tag{5}$$

$$V_{peak} = V_{phase} \times \sqrt{2} = 408.25\ kV \tag{6}$$

B. RESULTS OF SIMULATION CASE 2

In this simulation case, the behaviour of the installed NBD GIC mitigation systems and the efficacy of MOVs arresters used to protect the capacitor banks were investigated under a Single Line to Ground (SLG) fault in two simulation scenarios. Firstly, it was assumed that the GIC mitigation systems were set to the solid ground mode (the AC and DC switches assembly in the placed NBDs were in the closed position) during the faulty condition, as illustrated in Fig. 8(a). Then, the GIC protection modes in the NBDs were enabled (the AC and DC switch assembly were in the open position) and the simulation was repeated (Fig. 8(b)).

Additionally, proper settings (thresholds and time delays) were determined with no GIC flowing into transformers (all voltages representing the earth's surface potentials were set to zero magnitudes). The fault scenario was modelled using the available fault source in the PSCAD/EMTDC library and simultaneously applied to a primary terminal of transformers. The fault time was set to start at 1 second of simulation time and cleared after 0.1333 seconds. The SLG fault was considered the most common fault that occurs in Malaysia. According to the power utility company in Malaysia Tenaga Nasional Berhad (TNB) five-year tripping statistics (from 2001 to February 14, 2006), more than 90% of the tripping was caused by SLG fault [37]–[39]. Hence, this assessment was necessary to investigate the possible ferroresonance under faulty conditions and determine whether the situation could be aggravated by overvoltage despite the expected operation of the MOVs for these conditions. Besides, this assessment was performed to evaluate the energy handling capabilities of the MOVs used in NBDs since the MOV would fail to open if its energy limit is exceeded during the faulty condition, resulting in catastrophic overvoltage across the capacitors [22]. The applied fault current and instantaneous current and voltage at the HV side of 500/275 kV autotransformer at substation 21 are illustrated in Figs. 9 and 10.

The detailed results of the above tests for solid ground and GIC protection modes of NBDs during the faulty condition are presented in Figs. 11–13 and indicated as red and blue lines, respectively. Additionally, Fig. 11 depicts that the RMS

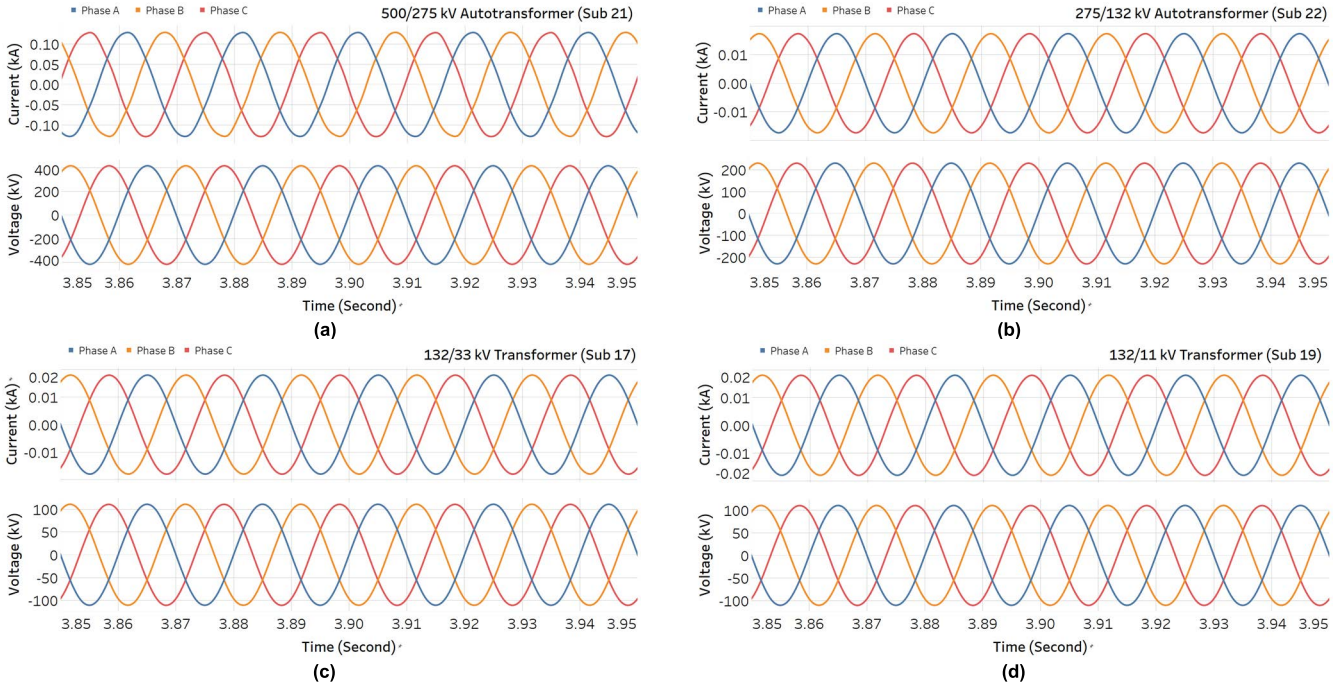

FIGURE 7. Three-phase current and voltage waveforms at the primary sides of different transformer types in the Malaysian power network under steady-state conditions at (a) substation 21, (b) substation 22, (c) substation 17, and (d) substation 19.

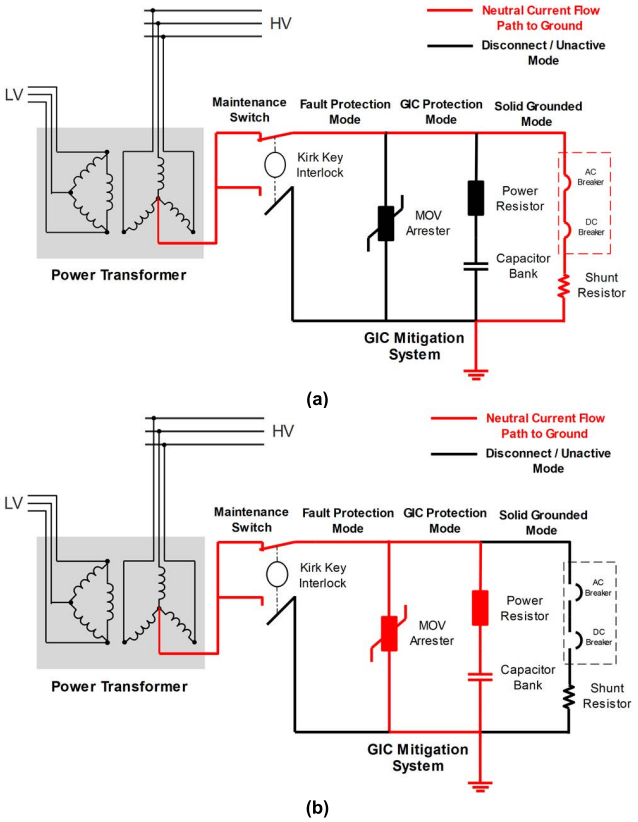

FIGURE 8. Mitigation system during a faulty condition when (a) solidly grounded and (b) GIC protection mode was enabled.

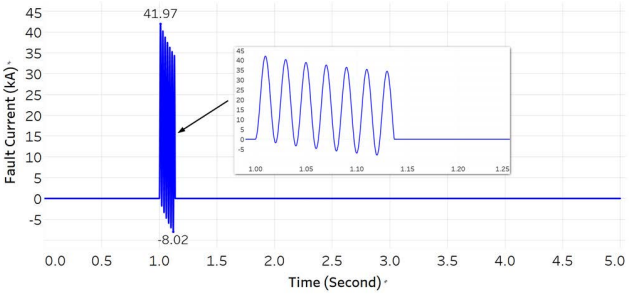

FIGURE 9. SLG applied fault current at the primary side of 500/275 kV autotransformer at substation 21.

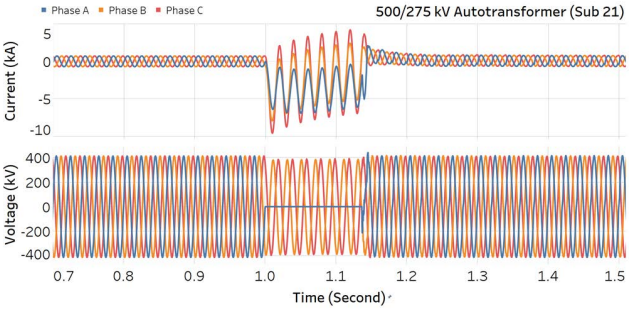

FIGURE 10. Three-phase current and voltage waveforms at the primary side of 500/275 kV autotransformer at substation 21 during the SLG fault.

voltages at the HV voltage sides of transformers dropped from 1 pu to below 0.78 pu during the faulty condition. The RMS voltages experienced the same drop rates for both solid ground and GIC protection modes of NBDs.

Meanwhile, Fig. 12 shows the neutral currents during the solid ground and GIC protection modes of NBDs in

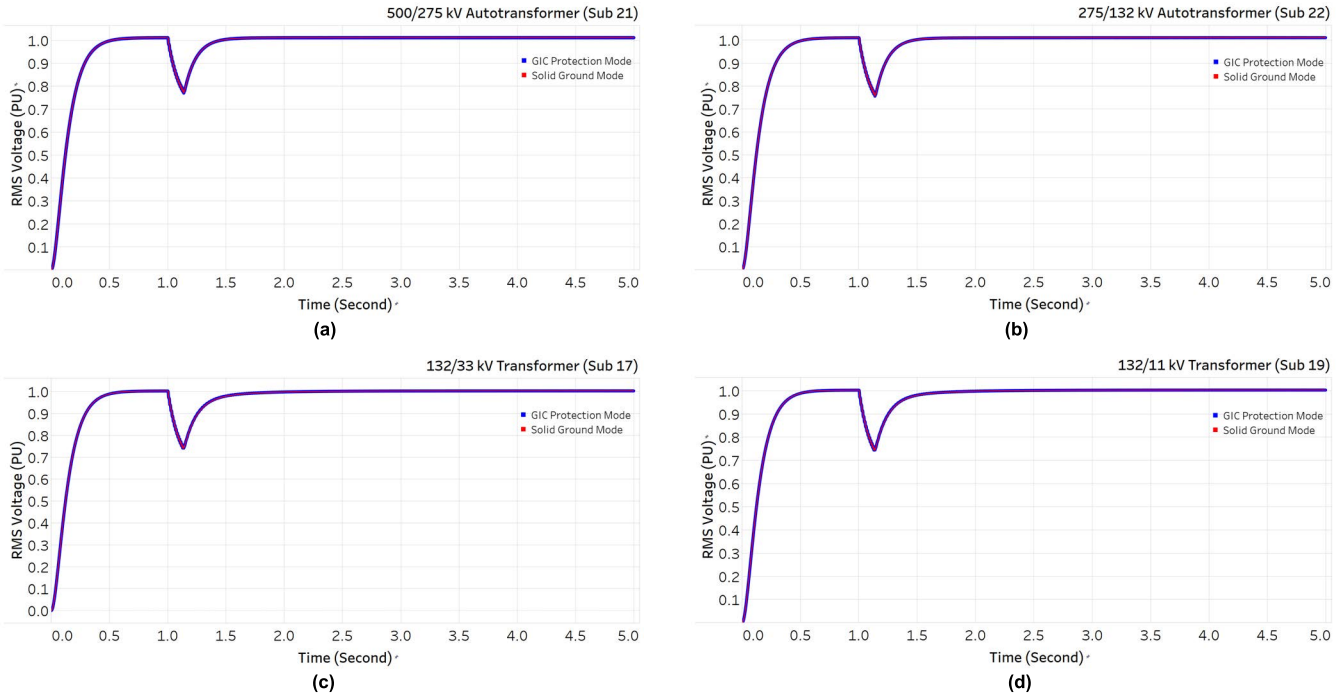

FIGURE 11. RMS voltages at the primary sides of different transformer types in the Malaysian power network under faulty conditions at (a) substation 21, (b) substation 22, (c) substation 17, and (d) substation 19.

substations 21, 22, 17, and 19. The results demonstrated that all components (the switches and the shunt resistors) in the solid ground mode and the MOV arresters in NBD mitigation systems passed this phase of testing. The conducted fault currents were cleared by the normal processes and at the same time protecting the capacitor banks from damage. However, the flowing currents during the GIC protection modes were slightly smaller due to the available impedance in their paths. Moreover, the graphs show that higher transformer MVA and kV ratings resulted in higher flowing fault currents in the neutrals. The largest fault current of 21.13 kA was observed at the neutral ground of the 500/275 kV autotransformer in substation 21 during the solid ground mode operation. In comparison, the lowest current of 1.01 kA was observed at the neutral ground path of 132/11 kV transformer in substation 19, as illustrated in Fig. 12(a) and (d).

In terms of the possible voltage build-up across the capacitors and potential ferroresonance during the ground faults, Fig. 13 shows that the solid ground mode operation of NBDs presented good control of overvoltages from the neutral to grounds, and the neutral voltages were close to zero. In this case scenario, the MOV arresters were not operated (triggered) since the neutral voltages were very small and did not exceed the arresters' clamping voltage level. However, a small current leakage in the milliampere range could still be observed in the arresters [40].

During the GIC protection mode, Fig. 13 shows that the connected arresters in the NBD systems were enabled and successfully clamped overvoltages in the neutral paths of transformers to below their protection levels of 3.67 kV and drained most of the fault currents that the system experienced. It should be noted that MOVs provide a low resistive path (typically 1–5 Ω) when entering the pressure relief mode. The highest clamped voltage variation was obtained in the 500/275 kV autotransformer in substation 21 at 3.26 kV given its highest neutral fault current, as illustrated in Figs.12(a) and 13(a). The developed voltage across the NBDs could be greater than the device rating, particularly when combined with the DC voltage caused by a GMD event [22]. These overvoltages in the neutrals of transformers during SLG faults and without MOVs were further discussed in the next simulation case. Regarding the potential effects due to the rapid collapse of the neutral voltage by MOV, two groups of researchers from the University of Manitoba and ASEA Brown Boveri (ABB) corporation have analysed the potential damage of transformer insulation when a MOV rapidly collapses the neutral voltage. The researchers found that this rapid change in the neutral voltage would not damage the insulation on the transformer windings [20].

In order to demonstrate the pressure relief process of the arresters and energy stress levels during the GIC protection modes, the flow of discharged fault current and energy dissipated through MOVs under faulty conditions were calculated and presented in Fig. 14. As depicted in the figure, when the faults started at 1 second, the MOVs were activated and drained the fault currents to the ground. The discharged highest current and dissipated energy through MOVs were observed at the NBD connected to the 500/275 kV autotransformer in substation 21 up to −19.82 kA and 3.206 MJ, respectively. At the NBD

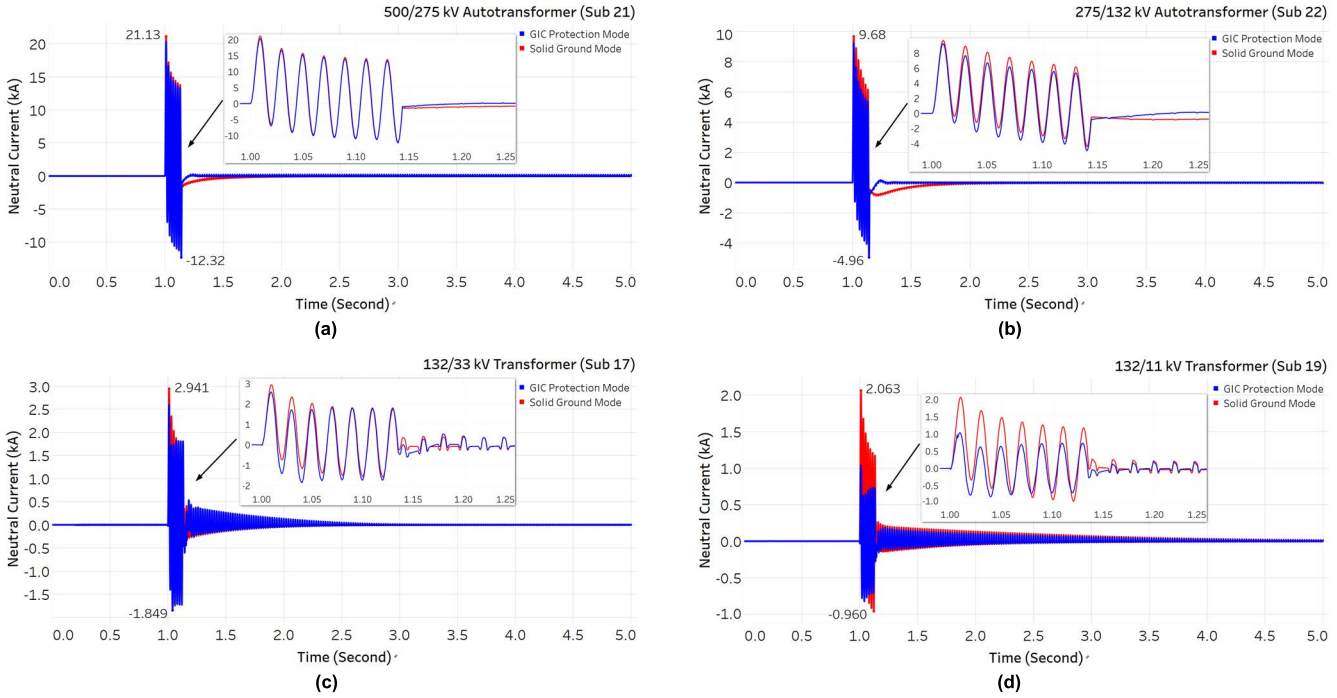

FIGURE 12. Neutral currents of different transformer types in the Malaysian power network under faulty conditions at (a) substation 21, (b) substation 22, (c) substation 17, and (d) substation 19.

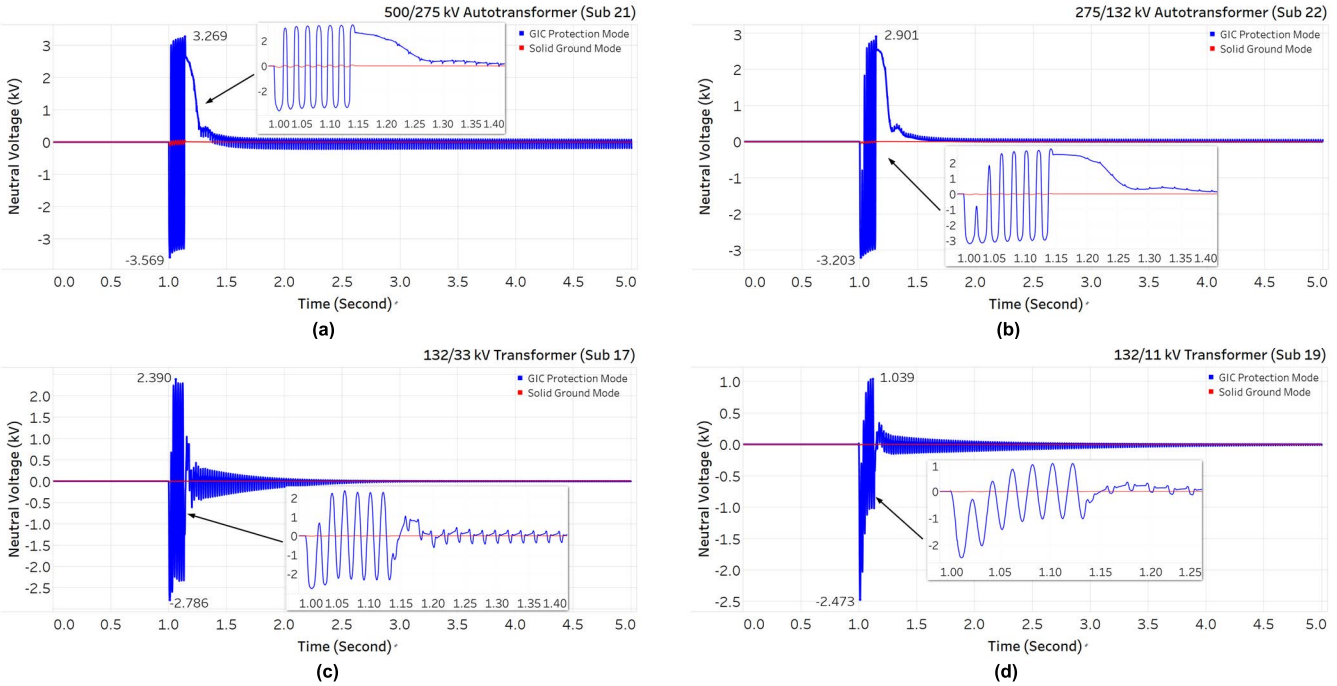

FIGURE 13. Neutral voltages of different transformer types in the Malaysian power network under faulty conditions at (a) substation 21, (b) substation 22, (c) substation 17, and (d) substation 19.

connected to the 275/132 kV autotransformer, the discharged current and dissipated energy variations through MOV were equal to −8.88 kA and 1.036 MJ. Whereas the discharged current and dissipated energy of the MOV in the connected NBD 132/33 kV transformer in substation 17 were equal to 2.072 kA and 60.92 kJ. The lowest current and energy dissipated through the MOV arrester in this simulation case obtained at the NBD connected to the 132/11 kV transformer were −0.388 kA and 4.368 kJ. As shown in the figure, the energy dissipation and current flow through the MOVs were increased when the fault current was increased. The dissipated energy of the arrester was computed based on Equation 7 [41].

$$W = \int_{t_0}^{t} u_A(t)\, i_A(t)\, dt \tag{7}$$

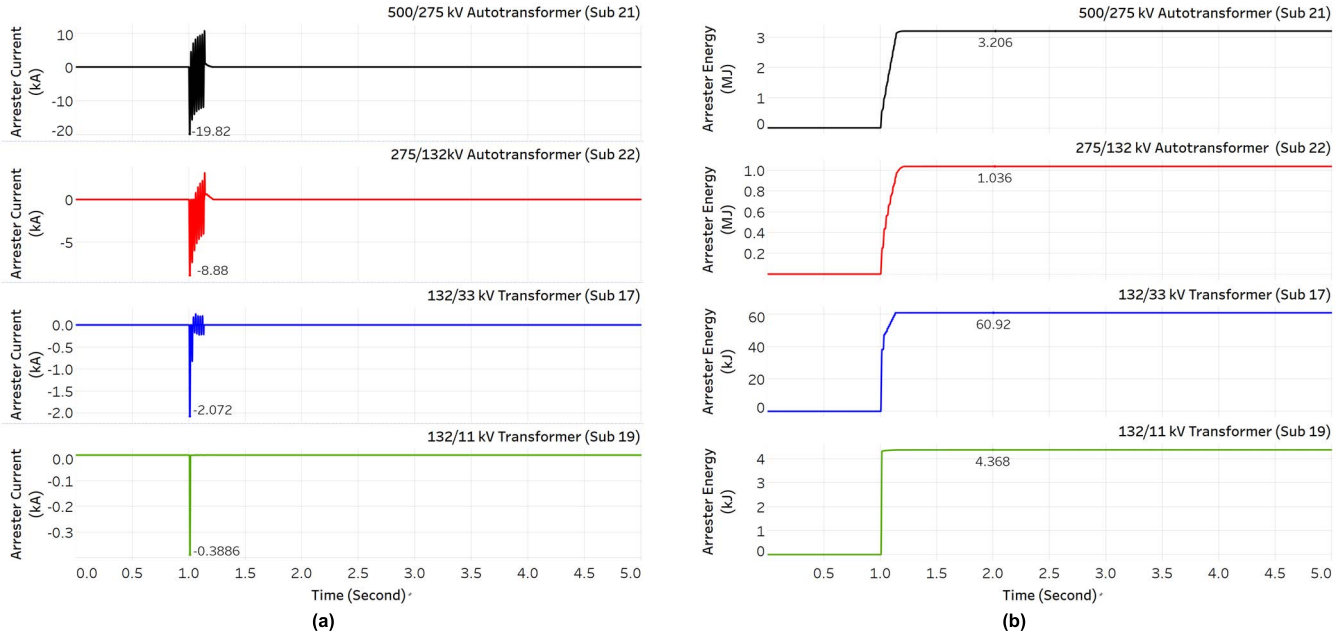

FIGURE 14. Simulation results of the MOV arresters in NBDs under faulty conditions (a) discharged current variations and (b) dissipated energy.

where W is the energy dissipated in the surge arrester during the discharge process, t_0 is the time instant when the surge current reaches the arrester, $u_A(t)$ and $i_A(t)$ are the instantaneous voltage and discharge current across the arrester, respectively. The results showed that connected NBDs to the higher kV and MVA rated transformers, such as substations 21, 22, and 17, required high-energy MOVs handling capabilities. If the MOV energy limit is exceeded, the MOV will fail to open during the faulty conditions, thus, leaving the NBD capacitor bank without HV protection. A failed MOV condition would result in severe overvoltage across the capacitor, which may cause major capacitor damage or even transformer insulation failure [22], [23]. Some utilities may connect an additional spark gap arrester parallel with the MOV in the NBD system to provide an extra conducting path to the ground and fault protection. Spark gap arresters have been shown as reliable, simple, low cost, low capacitance, and extremely high energy dissipation to handle very high currents [33]. The available arresters in the mitigation systems should be replaced only under rare circumstances since the occurrence of simultaneous faults during the GIC event was very rare [20].

C. RESULTS OF SIMULATION CASE 3

During the operation of installed NBD mitigation systems, the ground faults could result in ferroresonance overvoltage, while the transformer neutrals are in GIC protection modes due to the higher grounding impedance. Therefore, in this simulation case, the effects of power resistances and capacitances in the NBD systems on the ferroresonance overvoltage were investigated during the SLG fault in two simulation parts when these systems were in the GIC protection modes and MOVs were disconnected, as illustrated in Fig. 15.

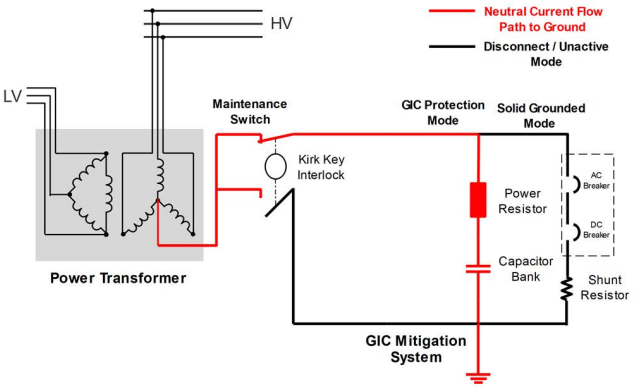

FIGURE 15. NBD system without the MOV connection.

In the first part of the simulation, the values of the capacitor banks were fixed at 3180 μF, while the connected power resistances in the GIC protection modes of the NBD systems were varied in the range of 1–4 Ω. The SLG faults were applied to the primary sides of the transformers at the NBDs-installed substations, and the neutral ground currents and voltages were measured for each value. Similarly to the previous case, the faults were set to occur after 1 second of simulation time and cleared after 0.1333 seconds.

For the second part of the simulation, the power resistances were fixed at 1 Ω, while the capacitances of capacitor banks were varied in the range of 31.8, 318.0, 3180, and 5300 μF. The simulation was repeated and the neutral ground current and voltage results were obtained due to the same applied faults for each capacitance value. These above-mentioned

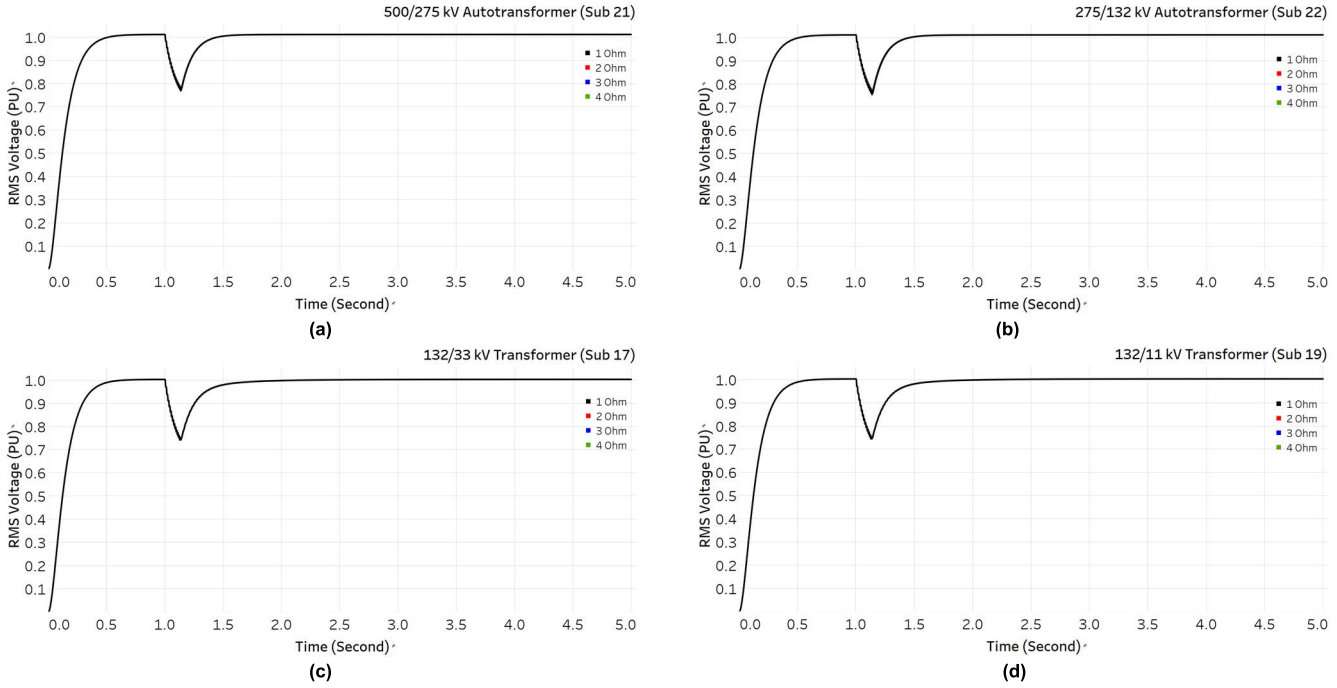

FIGURE 16. Variation of RMS voltages of transformers with different resistances under faulty conditions at (a) substation 21, (b) substation 22, (c) substation 17, and (d) substation 19.

values of series power resistor and capacitor bank available in the GIC NBD systems were selected randomly and based on the previous study [42]. Figs. 16–18 depict the results of the RMS voltages, neutral currents, and voltages of 500/275 kV, 275/132 kV, 132/33 kV, and 132/11 kV transformers in substations 21, 22, 17, and 19 for the first part of the simulation, respectively. The results of 1, 2, 3, and 4 Ω were represented in the graphs as black, red, blue, and green, respectively.

Fig. 16 shows that similar values of RMS voltages were obtained at the HV sides of transformers due to various power resistances with the same voltage drops. The graphs overlapped each other since they had similar results. The RMS voltages of transformers dropped from 1 pu to below 0.78 pu when the fault currents were applied at 1 second.

Furthermore, Fig. 17 shows that the neutral currents in the neutral paths of transformers slightly decreased by the increase in the power resistances of the connected mitigations systems under faulty conditions since they were supposed to limit the current flows. The highest variations of neutral currents were obtained at 1 Ω, while the lowest variations were obtained at 4 Ω.

Contrary to the neutral currents, Fig. 18 shows that by increasing the power resistances of the connected NBDs, the neutral voltages of transformers increased during the faulty condition. Fig.18(a) shows that the maximum variation of neutral voltage in the neutral path of the 500/275 kV autotransformer was in the range of 43.8 to −58.2 kV when the power resistance was 4 Ω, while the minimum variation was in the range of 20.5 to −43.7 kV when the power resistance was 1 Ω. Additionally, the maximum variation in the neutral of 275/132 kV autotransformer was in the range of 22.86 to −40.10 kV for a 4 Ω resistance, while the minimum variation was in the range of 11.05 to −27.44 kV when the resistance was 1 Ω (Fig.18(b)). Regarding the 132 kV transformers, the maximum variations of the resonant voltages in the 132/33 kV and 132/11 kV transformers were equal from 7.06 to −10.81 kV and 1.72 to −3.84 kV, respectively, for a 4 Ω power resistance, as illustrated in Fig.18(c) and (d). These values decreased from 3.75 to −7.25 kV and 1.15 to −3.03 kV when the power resistance decreased to 1 Ω in both transformers, respectively. This analysis showed that the 1 Ω resistor in series with the capacitor bank effectively dampened the potential resonances caused by the neutral connection. In other words, a higher value of series power resistor in a mitigation system might increase the potential ferroresonance.

Figs. 19–21 depict the results of the RMS voltages, neutral currents, and voltages of transformers for the second part of the simulation when the value of power resistors in the NBDs were fixed to 1 Ω, whereas the values of the capacitor banks were varied at 31.8, 318.0, 3180, and 5300 μF, which were represented as black, red, blue, and green lines, respectively, in the graphs.

Fig. 19 depicts that the drop in RMS voltages during the applied faults at the primary sides of transformers decreased slightly due to the decrease in the capacitance of the capacitor banks from the connected NBDs. For example, in the 500/275 kV autotransformer located in substation 21, the RMS voltage dropped from 1 pu to 0.76 pu during a faulty condition and when the grounding capacitances were equal to 318, 3180, and 5300 μF (Fig. 19(a)). This drop rate was reduced to 0.80 pu when the grounding capacitance

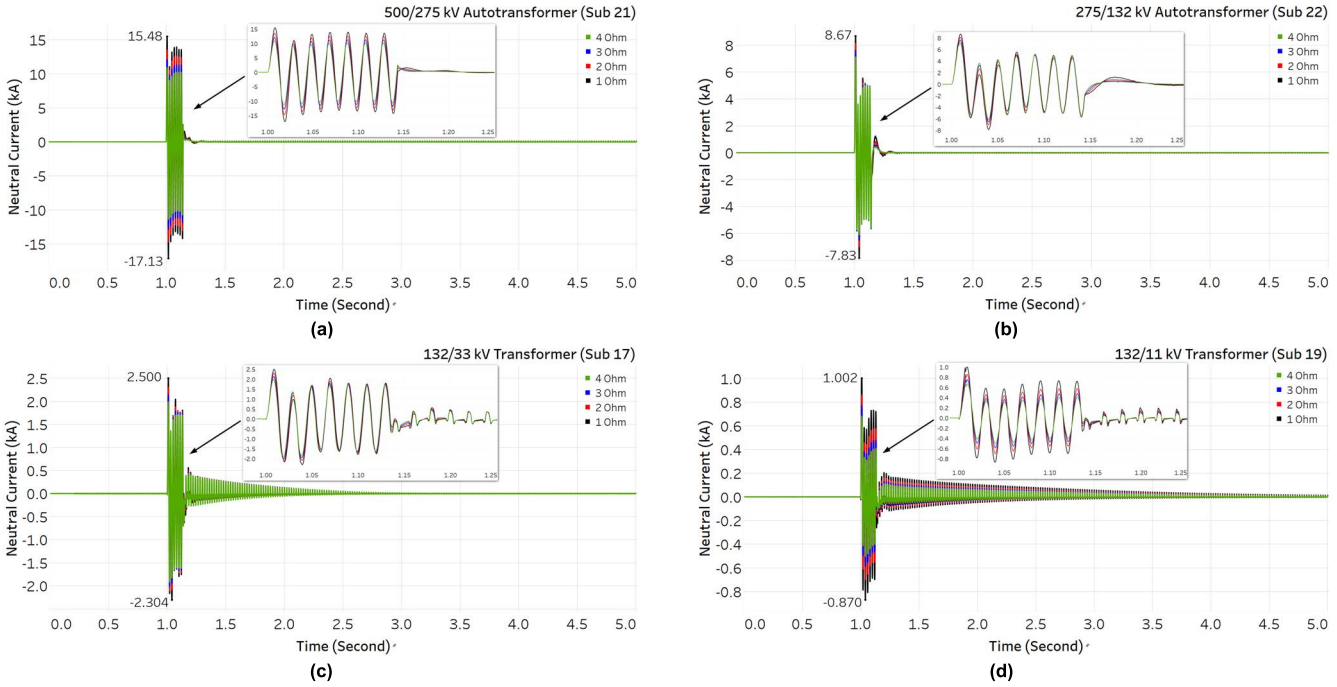

FIGURE 17. Variation of neutral currents of transformers with different resistances under faulty conditions at (a) substation 21, (b) substation 22, (c) substation 17, and (d) substation 19.

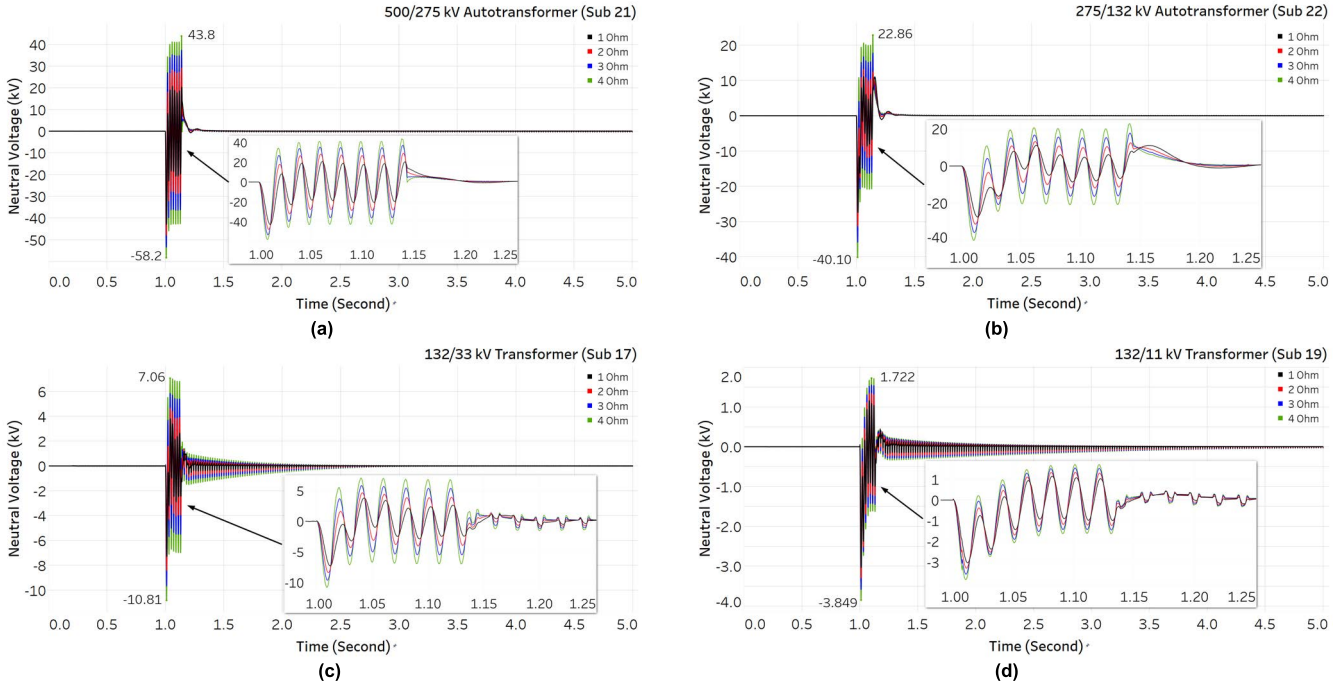

FIGURE 18. Variation of neutral voltages of transformers with different resistances under faulty conditions at (a) substation 21, (b) substation 22, (c) substation 17, and (d) substation 19.

was decreased to 31.8 μF under the same applied faulty condition. The highest RMS voltage drop differences were obtained by the 275/132 kV autotransformer in substation 22. As shown in Fig. 19(b), when the grounding capacitance was equal to 318, 3180, and 5300 μF, the RMS voltage dropped from 1 pu to 0.75 pu. However, when the grounding capacitance was decreased to 31.8 μF, the drop rate was reduced to 0.83 pu. The RMS voltage results in the 132/33 kV and 132/11 kV transformers were almost similar for different grounding capacitances under each faulted current with similar values compared to the previous simulation cases (Fig. 19(c) and (d)).

In terms of the neutral currents, different variation rates were obtained with respect to the different capacitor bank

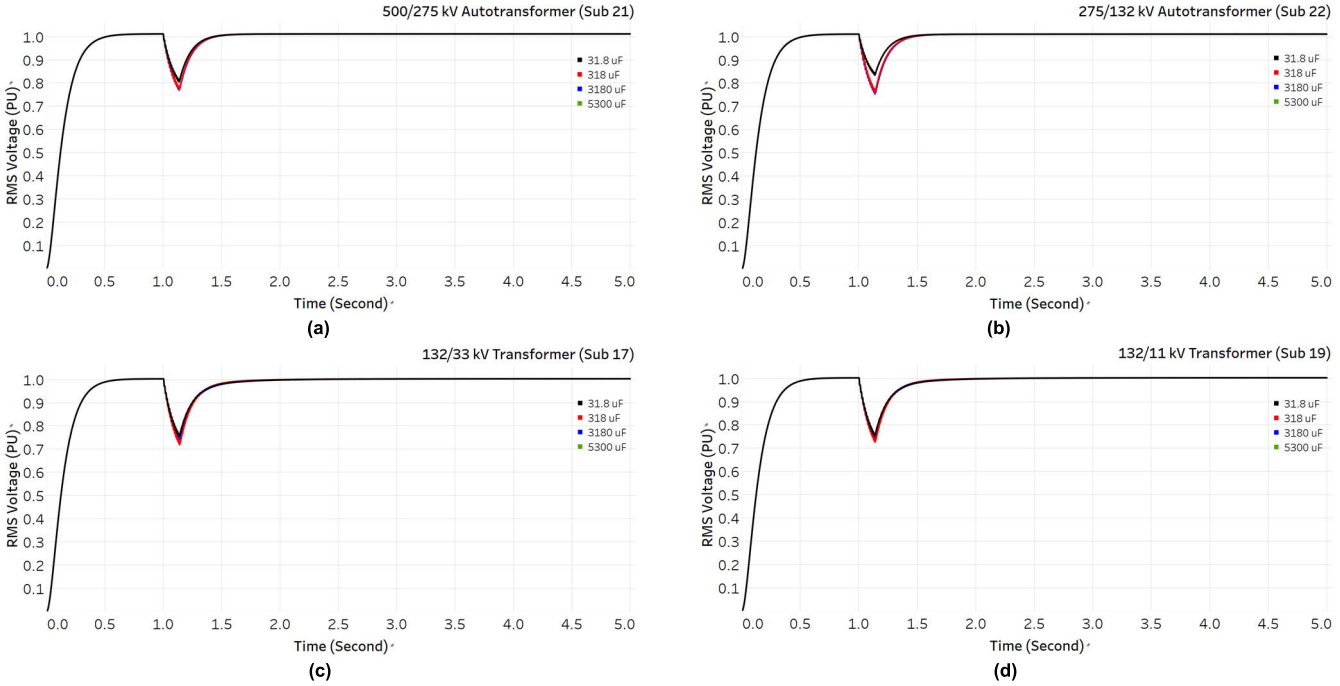

FIGURE 19. Variation of RMS voltages of transformers with different capacitances under faulty conditions at (a) substation 21, (b) substation 22, (c) substation 17, and (d) substation 19.

values and transformer types, as illustrated in Fig. 20. For instance, in Fig. 20(a), the maximum current variation in the ground path of 500/275 kV autotransformer was in the range of 16.31 to −17.13 kA when the capacitance of the capacitor bank was equal to 5300 and 3180 μF, respectively, during the applied faulty condition. The value range was decreased slightly and became 14.25 to −14.21 kA when the capacitance decreased to 318 μF. Furthermore, the minimum variation of neutral current was in the range of 1.81 to −1.30 kA when the grounding capacitance equals 31.8 μF. The maximum variation of neutral currents obtained in the 275/132 kV autotransformer and 132/33 kV transformer were in the ranges of 19 to −19.43 kA and 7.91 to −7.78 kA, respectively, when the grounding capacitances were equal to 318 μF. In contrast, the minimum variations were obtained with values of 1.49 to −1.35 kA and 1.11 to −1.04 kA for both transformers, respectively, when the grounding capacitances were equal to 31.8 μF (Fig. 20(b) and (c)). In Fig. 20(d), the maximum variation of neutral current in the 132/11 kV transformer was obtained in the range of 1.15 to −0.90 kA when the grounding capacitance was equal to 5300 μF, while the neutral current was close to zero when the capacitance was equal to 31.8 μF.

Fig. 21 illustrates the variations of resonant overvoltages in the neutral paths of the transformers, where the NBD systems were connected under faulty conditions. From the figure, the lowest variations were obtained when the values of these capacitors were set to 5300 μF. In contrast, the highest overvoltage occurred when the capacitance of capacitor banks was set to 318 and 31.8 μF. For example, in Fig. 21(a), the minimum resonant overvoltage variation in the 500/275 kV autotransformer was in the range of 15.5 to −33.7 kV when the grounding capacitance was 5300 μF. The value was then increased at a range of 140.3 to −139.4 kV, which was approximately four times greater when the capacitance was decreased to 318 μF. The ground overvoltage was decreased at a range of 119.9 to −125.1 kV when the grounding capacitance was reduced to 31.8 μF. The finding indicates that decreasing the capacitance of the capacitor bank would not always increase the resonant overvoltages. It was worth mentioning that the GIC blocking capacitor bank values in previous cases were set to 3180 μF. In the 275/132 kV autotransformer, the minimum variation was in the range of 7.6 to −19.9 kV for the 5300 μF capacitance, while the maximum variation was in the range of 189.7 to −191.5 kV, which was approximately nine times greater for the 318 μF capacitance. This variation was considered the highest value among the overvoltage results in the transformer's ground (Fig. 21(b)). In addition, Fig. 21(c) depicts that the resonant overvoltage in the neutral of 132/33 kV transformer due to the applied fault still had a large variation with a value of 80.7 to −76.1 kV when the grounding capacitance was 318 μF.

In contrast, the minimum value was obtained with a value of 2.6 to −5.8 kV when the capacitance was 5300 μF. However, the 31.8 μF capacitor bank developed a high oscillation after the ground faults ended at 1.6 seconds and continued until 3.7 seconds of the simulation time. In the 132/11 kV transformer, the results of overvoltage for different capacitor values were considered small compared to other transformers with a 31.8 μF capacitance recorded the maximum

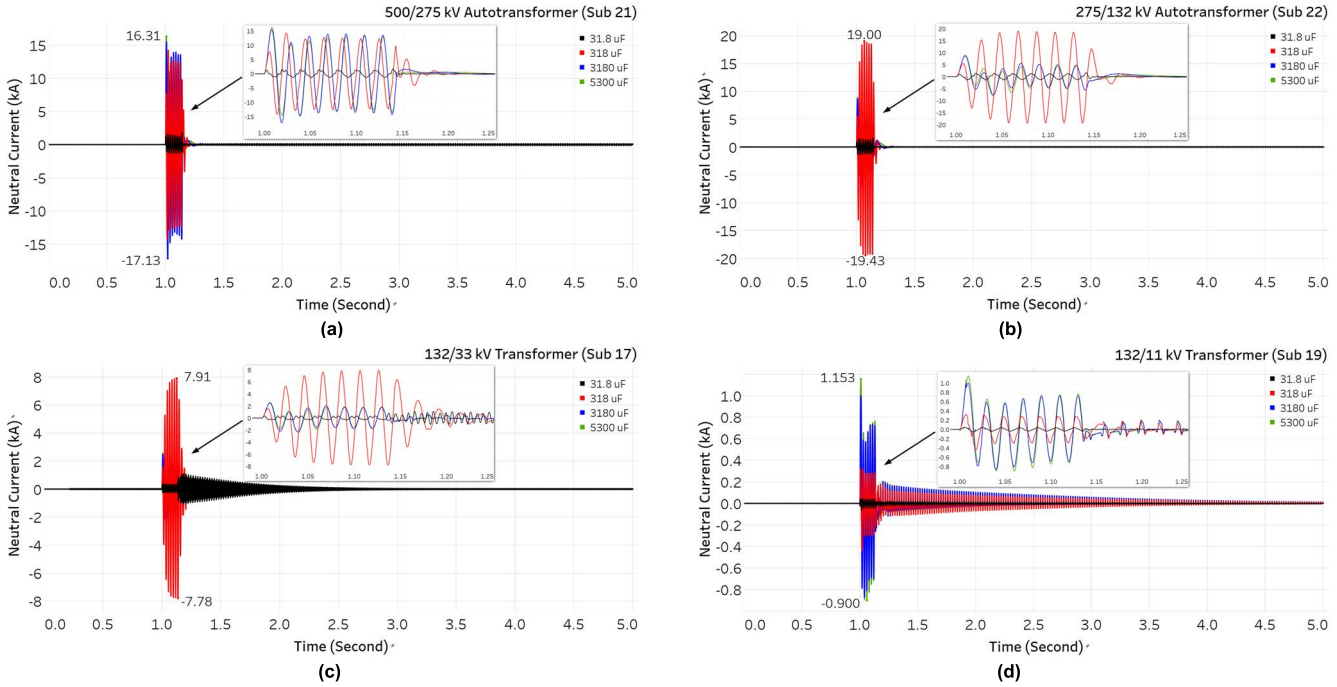

FIGURE 20. Variation of the neutral currents of transformers with different capacitances under faulty conditions at (a) substation 21, (b) substation 22, (c) substation 17, and (d) substation 19.

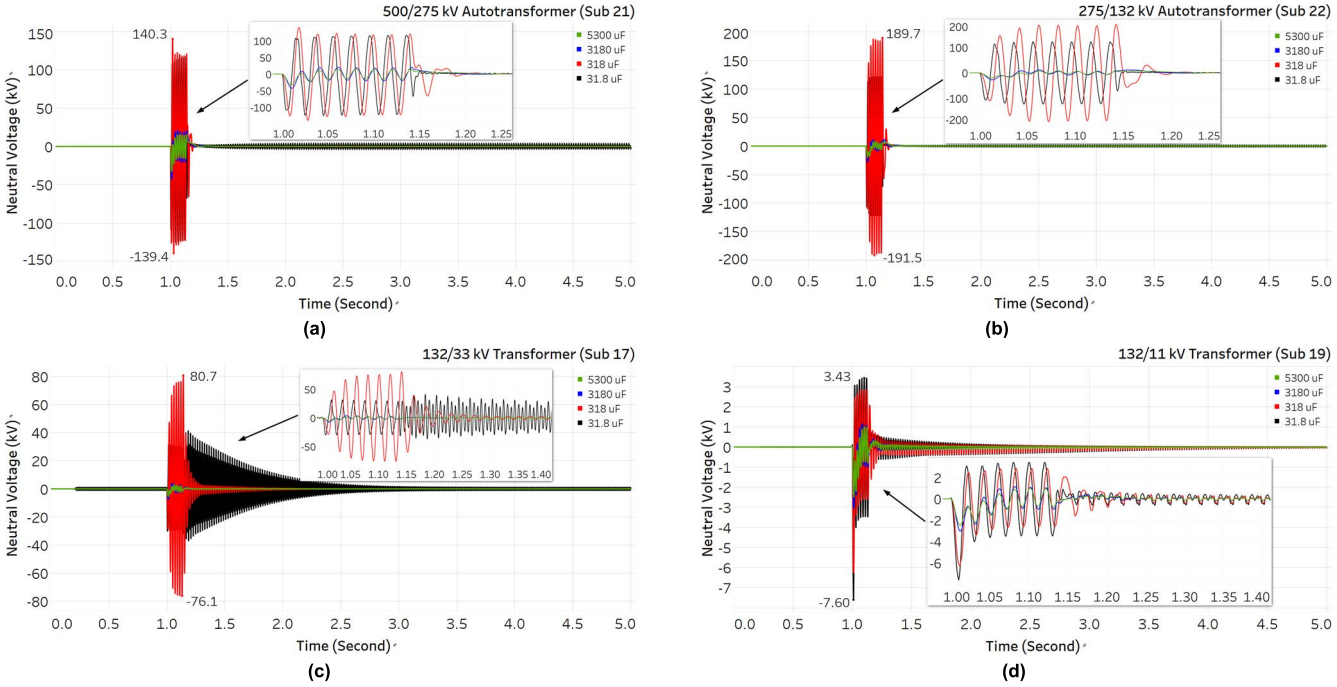

FIGURE 21. Variation of neutral voltages of transformers with different capacitances under faulty conditions at (a) substation 21, (b) substation 22, (c) substation 17, and (d) substation 19.

variation of 3.43 to −7.60 kV (Fig. 21(d)). Overall, the results showed that the resonance overvoltage could be increased by decreasing the capacitance of capacitor banks. However, the increase rate varies from one transformer to another. Also, the results of this simulation case demonstrated that the amplitudes of overvoltages that were developed in the neutral paths of transformers during SLG faults when the GIC protection modes of NBDs were enabled and MOVs were disconnected. The obtained overvoltages in most cases were large enough to damage capacitor banks and windings of transformers. This scenario simulated the case when connected MOVs fail to open under faulty conditions. Therefore, when a neutral blocking system is implemented, it is recommended to conduct a simulation analysis or laboratory test to evaluate the potential resonance overvoltage across the capacitor banks during faulty conditions, especially when the

mitigation system is in the GIC protection mode. Given that the increased overvoltage may exceed the energy handling limits of MOVs used to protect capacitor banks, as discussed in the previous simulation case, therefore, additional protection against ferroresonance events should be possible by adding a relay capable of sensing such resonance and bypassing the capacitor [20].

IV. CONCLUSION

This study investigated the effect of GIC NBD systems on the power network ferroresonance in Malaysia. The Malaysian power network and NBDs were modelled by using the PSCAD software. The connected NBD systems to the transformers have been evaluated under SLG faults with respect to different working scenarios with and without MOVs connection. The available MOVs that were used to protect the capacitor banks in the NBD systems could suppress overvoltage in the neutral grounds during faulty events. Nevertheless, high variations of dissipated current and energy were observed through MOVs in the NBDs that were connected to transformers in substations 21, 22, and 17 since these transformers possessed higher MVA and kV ratings. The analysis showed that the 1 Ω series power resistors and 3180 μF (1 Ω impedance) capacitor banks in the mitigation systems effectively dampened the potential ferroresonance caused by the neutral connection. Based on the overall analysis results that were obtained in this work, the following recommendations are given to the local power utility.

1) Before a GIC mitigation system installation, it is recommended to perform a simulation analysis or laboratory test to assess the potential resonance overvoltage across the power capacitors during a faulty condition when this system is in the GIC protection mode.
2) MOVs connected to high MVA rating transformers must be equipped with high-energy handling capabilities or be connected to additional spark gap arresters in parallel to avoid any failure and ensure the protection of capacitor banks from severe overvoltage in the system during ferroresonance phenomena or faulty conditions.
3) The values of series resistors and capacitor banks in the mitigation systems should be 1 Ω and 3180 μF, respectively.

REFERENCES

[1] M. Wik, R. Pirjola, H. Lundstedt, A. Viljanen, P. Wintoft, and A. Pulkkinen, "Space weather events in July 1982 and October 2003 and the effects of geomagnetically induced currents on Swedish technical systems," *Ann. Geophys.*, vol. 27, no. 4, pp. 1775–1787, 2009.

[2] D. M. Oliveira and C. M. Ngwira, "Geomagnetically induced currents: Principles," *Brazilian J. Phys.*, vol. 47, no. 5, pp. 552–560, Oct. 2017.

[3] S. P. Blake, P. T. Gallagher, J. McCauley, A. G. Jones, C. Hogg, J. Campanyà, C. D. Beggan, A. W. P. Thomson, G. S. Kelly, and D. Bell, "Geomagnetically induced currents in the Irish power network during geomagnetic storms," *Space Weather*, vol. 14, no. 12, pp. 1136–1154, Dec. 2016.

[4] C. M. Ngwira, A. Pulkkinen, M. M. Kuznetsova, and A. Glocer, "Modeling extreme 'Carrington-type space weather events using three-dimensional global MHD simulations," *J. Geophys. Res., Space Phys.*, vol. 119, no. 6, pp. 4456–4474, 2014.

[5] J. Ramírez-Niño, C. Haro-Hernández, J. H. Rodriguez-Rodriguez, and R. Mijarez, "Core saturation effects of geomagnetic induced currents in power transformers," *J. Appl. Res. Technol.*, vol. 14, no. 2, pp. 87–92, Apr. 2016.

[6] R. Pirjola and D. Boteler, "Geomagnetically induced currents in European high-voltage power systems," presented at the Canadian Conf. Elect. Comput. Eng., Ontario, ON, Canada, 2006.

[7] M. Heindl, M. Beltle, M. Reuter, D. Schneider, S. Tenbohlen, D. T. Oyedokun, and C. T. Gaunts, "Investigation of GIC related effects on power transformers using modern diagnostic methods," in *Proc. Int. Symp. High Voltage Eng.*, Hannover, Germany, Aug. 2011, pp. 1–6.

[8] R. Zhang, "Transformer modelling and influential parameters identification for geomagnetic disturbances events," Doctor Philosophy, Dept. Elect. Electron. Eng., Univ. Manchester, U.K., 2012.

[9] C. Liu, Y. Li, and R. Pirjola, "Observations and modeling of GIC in the Chinese large-scale high-voltage power networks," *J. Space Weather Space Climate*, vol. 4, p. A03, Jan. 2014.

[10] O. Samuelsson, *Geomagnetic Disturbances and Their Impact on Power Systems*. Lund, Sweden: Lund Univ., 2013.

[11] F. Aboura and O. Touhami, "Effect of the GICs on magnetic saturation of asymmetric three-phase transformer," *IET Electr. Power Appl.*, vol. 11, no. 7, pp. 1306–1314, Aug. 2017.

[12] T. Hutchins, "Geomagnetically induced currents and their effect on power systems," M.S. thesis, Dept. Elect. Comput. Eng., Univ. Illinois Urbana-Champaign, Champaign, IL, USA, 2012.

[13] R. Caraballo, "Geomagnetically induced currents in uruguay: Sensitivity to modelling parameters," *Adv. Space Res.*, vol. 58, no. 10, pp. 2067–2075, Nov. 2016.

[14] C.-M. Liu, L.-G. Liu, and R. Pirjola, "Geomagnetically induced currents in the high-voltage power grid in China," *IEEE Trans. Power Del.*, vol. 24, no. 4, pp. 2368–2374, Oct. 2009.

[15] R. P. Jayasinghe, "Investigation of protection problems due to geomagnetically induced currents," Doctor Philosophy, Dept. Elect. Comput. Eng. Univ. Manitoba Canada, Winnipeg, MB, Canada, 1996.

[16] Z. M. K. Abda, N. F. A. Aziz, M. Z. A. A. Kadir, and Z. A. Rhazali, "A review of geomagnetically induced current effects on electrical power system: Principles and theory," *IEEE Access*, vol. 8, pp. 200237–200258, 2020.

[17] S. Kim, B. Sung, S. Kim, Y. Choi, and H. Kim, "A study on ferroresonance mitigation techniques for power transformer," in *Proc. Int. Conf. Power Syst. Transients (IPST)*, Jun. 2015, pp. 1–7.

[18] B. Baldwin, S. Sabade, and S. Joshi, *A Study of Ferroresonance & Mitigation Techniques*. Houghton, MI, USA: Michigan Tech, 2013.

[19] A. Shemshadi and P. Khorampour, "The investigation of ferro resonance voltage fluctuation considering load types and damping factors," *Energy Harvesting Syst.*, 2022.

[20] F. R. Faxvog, W. Jensen, G. Fuchs, G. Nordling, D. B. Jackson, B. Groh, N. Ruehl, A. P. Vitols, T. L. Volkmann, M. R. Rooney, and R. Neal, "Power grid protection against geomagnetic disturbances (GMD)," in *Proc. IEEE Electr. Power Energy Conf.*, Aug. 2013, pp. 1–13.

[21] A. D. Rajapakse, N. Perera, F. R. Faxvog, W. Jensen, G. Nordling, G. Fuchs, D. B. Jackson, T. L. Volkmann, N. Ruehl, and B. Groh, "Power grid stability protection against GIC using a capacitive grounding circuit," in *Proc. PES (T&D)*, May 2012, pp. 1–6.

[22] H. A. Saeed, "Effects of GIC neutral blocking devices (NBDs) on transmission lines protection performance and potential for resonance," M.S. thesis, Dept. Elect. Eng., Univ. Tennessee Chattanooga, Chattanooga, TX, USA, 2015.

[23] T. C. Akinci, N. Ekren, S. Seker, and S. Yildirim, "Continuous wavelet transform for ferroresonance phenomena in electric power systems," *Int. J. Electr. Power Energy Syst.*, vol. 44, no. 1, pp. 403–409, Jan. 2013.

[24] T. A. Mellik, F. D. Painter, D. D. Shipp, and T. J. Dionise, "Proactive study and novel mitigation of MV power system damage due to sub-power-frequency ferro-resonance for a gas plant," *IEEE Trans. Ind. Appl.*, vol. 54, no. 4, pp. 3991–4000, Jul. 2018.

[25] R. C. Dugan, M. F. M. Granaghan, S. Santoso, and H. W. Beaty, *Electric Power Systems Quality*. New York, NY, USA: McGraw-Hill, 2004.

[26] B. Behdani, M. Allahbakhshi, and M. Tajdinian, "On the impact of geomagnetically induced currents in driving series capacitor compensated power systems to ferroresonance," *Int. J. Electr. Power Energy Syst.*, vol. 125, Feb. 2021, Art. no. 106424.

[27] J. E. Berge, "Impact of geomagnetically induced currents on power transformers," Doctor Philosophy, Dept. Elect. Comput. Eng., Univ. Western Ontario, Toronto, ON, Canada, 2011.

[28] T. Halbedl, "Low frequency neutral point currents on transformer in the Austrian power transmission network," Ph.D. dissertation, Inst. Elect. Power Syst., Graz Univ. Technol., Graz, Austria, 2019.
[29] J. A. Martinez-Velasco and F. González-Molina, *Temporary Overvoltages in Power Systems*, 2012.
[30] Z. M. Khurshid, N. F. A. Aziz, Z. A. Rhazali, and M. Z. A. A. Kadir, "Impact of geomagnetically induced currents on high voltage transformers in Malaysian power network and its mitigation," *IEEE Access*, vol. 9, pp. 167204–167217, 2021.
[31] O. Anaya-Lara and E. Acha, "Modeling and analysis of custom power systems by PSCAD/EMTDC," *IEEE Trans. Power Del.*, vol. 17, no. 1, pp. 266–272, Jan. 2002.
[32] PSCAD. (2021). *PSCAD Professional/Commercial, Educational, Trial, and Free Editions*. Manitoba Hydro International (MHI) Ltd. Accessed: Oct. 27, 2021. [Online]. Available: https://www.pscad.com/knowledge-base/article/52
[33] Z. Mohammed, "Lightning-induced transient effect in a hybrid PV-wind system and its Mitigation," M.S. thesis, Dept. Elect. Electron. Eng., Univ. Putra Malaysia, Seri Kembangan, Malaysia, 2018.
[34] T. N. Berhad, *Transmission System Reliability Standards*. Seri Kembangan, Malaysia: Tenaga Nasional Berhad, 2006.
[35] T. N. Berhad. (2020). *Grid Code for Peninsular Malaysia*. Malaysia. [Online]. Available: https://www.gso.org.my/GridCode/GridCode.aspx
[36] F. T. Sabah, T. Labuan, and N. Berhad. (2017). *Distribution Code for Peninsular Malaysia*. [Online]. Available: https://www.st.gov.my/en/contents/publications/guidelines_electricity/2017/Distribution%20Code%20For%20Peninsular%20Malaysia%20Sabah%20%20F.T.%20Labuan%20Amendments%202017_V5.pdf#:~:text=The%20amendments%20of%20the%20Distribution,other%20distributed%20generation%20into%20the
[37] S. H. Asman, N. F. Ab Aziz, M. Z. A. Abd Kadir, and U. A. U. Amirulddin, "Fault signature analysis based on digital fault recorder in Malaysia overhead line system," in *Proc. IEEE Int. Conf. Power Energy (PECon)*, Dec. 2020, pp. 188–193.
[38] A. A. M. Zin and S. P. A. Karim, "The application of fault signature analysis in tenaga nasional berhad Malaysia," *IEEE Trans. Power Del.*, vol. 22, no. 4, pp. 2047–2056, Oct. 2007.
[39] M. H. Idris, M. W. Mustafa, and Y. Yatim, "Effective two-terminal single line to ground fault location algorithm," in *Proc. IEEE Int. Power Eng. Optim. Conf.*, Jun. 2012, pp. 246–251.
[40] Z. Mohammed, H. Hizam, and C. Gomes, "Lightning-induced transient effects in a hybrid PV–wind system and mitigation strategies," *Electr. Power Syst. Res.*, vol. 174, Sep. 2019, Art. no. 105882.
[41] S. Milan, "Selection of the surge arrester energy absorption capability relating to lightning overvoltages," in *Proc. 18th Int. Conf. Exhib. Electr. Distrib. (CIRED)*, 2005, pp. 1–3.
[42] A. D. Rajapakse and N. Perera, "Simulation of transformer GIC mitigation using neutral DC current and voltage harmonic level to switch in a capacitor to the grounding circuit," in *Final Report Submitted to EMPRIMUS LLC*. Ottawa, ON, Canada, 2011.

ZMNAKO MOHAMMED KHURSHID received the Technical Diploma degree in electrical from the Kalar Technical Institute, Iraq, in 2007, the B.Eng. degree in electrical and electronic engineering from the Asia Pacific University of Technology & Innovation (APU), Malaysia, in 2015, the M.Sc. degree from Universiti Putra Malaysia (UPM), Malaysia, in 2018, and the Ph.D. degree in electrical engineering from Universiti Tenaga Nasional (UNITEN), Malaysia, in 2022. His current research interests include hybrid systems, particularly that contain renewable energy—PV systems and wind turbines, lightning and lightning transient effects, and geomagnetically induced current (GIC) on electrical power systems.

NUR FADILAH AB AZIZ (Member, IEEE) received the master's degree (Hons.) in electrical engineering from the University of Southampton, U.K., in 2006, and the Ph.D. degree from Universiti Teknologi Mara, Shah Alam, in 2014. She is currently a Senior Lecturer with the Department of Electrical and Electronics Engineering, Universiti Tenaga Nasional (UNITEN), Malaysia. Her research interests include power system analysis, renewable energy, fault identification and location, distribution automation, statistical pattern recognition, artificial intelligent (AI), and machine learning application in power systems. She is a Graduate Member with the Board of Engineers Malaysia (BEM).

ZETI AKMA RHAZALI received the bachelor's degree in electrical, electronics and system engineering from Universiti Kebangsaan Malaysia and the Ph.D. degree in electrical engineering from Universiti Malaysia Pahang, in 1996 and 2014, respectively. She was a Senior Engineer (Research and Development), from 1996 to 2001, with vast experiences in telecommunication technologies and advancements related to mobile radio, space, and satellite communications. She was the Head of the Department of Electronic and Communication Engineering, College of Engineering, Universiti Tenaga Nasional (UNITEN), from 2018 to 2019, where she is currently the Head of the Department of Engineering Foundation and Diploma Studies. She is a Professional Engineer (P.Eng.) registered with the Board of Engineers Malaysia (BEM). Her research interests include antenna synthesis and analyses, microwave and milimeter wave engineering, and ionospheric communication studies. She is a member with The Institution of Engineers (IEM), Malaysia.

MOHD ZAINAL ABIDIN AB KADIR (Senior Member, IEEE) received the B.Eng. degree in electrical and electronic engineering from Universiti Putra Malaysia and the Ph.D. degree in high voltage engineering from the University of Manchester, U.K., respectively. Currently, he is a Strategic Hire Professor with the Institute of Power Engineering (IPE), Universiti Tenaga Nasional (UNITEN), and a Professor with the Faculty of Engineering, Universiti Putra Malaysia, where he is the Founding Director of the Centre for Electromagnetic and Lightning Protection Research (CELP). He is an IEEE Power & Energy Society (PES) Distinguished Lecturer in lightning and high voltage engineering. He is a Professional Engineer (P.Eng.), a Chartered Engineer (C.Eng.), and a Professional Technologist (P.Tech.). He has authored and coauthored over 350 journals and conference papers. His research interests include high voltage engineering, lightning protection, electromagnetic compatibility, power system transients, and renewable energy. He is also an Advisory Board Member with the National Lightning Safety Institute (NLSI), USA, and a Research Advisor with the African Centre for Lightning and Electromagnetic (ACLE). Currently, he is the Chairperson of the National Mirror Committee of IEC TC 81 (Lightning Protection) and a Local Convener of MNC-CIGRE C4 on System Technical Performance.